Study of negative ion beamlets produced in SPIDER by Beam Emission Spectroscopy

R. Agnello, M. Barbisan, G. Casati, R. Pasqualotto, G. Serianni, B. Zaniol

***Abstract*—Among the beam diagnostics routinely employed in SPIDER, Beam Emission Spectroscopy (BES) provides valuable information for beam characterization, thus driving source optimization methods. In particular, this technique is used to measure beam divergence and uniformity, which are crucial parameters to be optimized for application in ITER. In this contribution, we focus on the characterization of $\mathrm{H}^-/\mathrm{D}^-$ beamlets extracted during the first SPIDER Cs campaigns. In particular, we show parametric scans and preliminary broad component estimates on single beamlets.**

I. Introduction

THE Heating Neutral Beam (HNB) injector designed for ITER is based on the injection of beams of H/D atoms delivering a power of 16.7 MW with particles accelerated up to 0.87 MeV for H and 1 MeV for D [1]. Nowadays, the most efficient technology to produce high energy ($> 100\,\mathrm{keV}$) atomic beams is based on the acceleration of $\mathrm{H}^-/\mathrm{D}^-$ ions and neutralization by electron stripping process with a background gas along the propagation direction. The target extracted current density for the ITER HNB injector is 350 $\mathrm{A/m^2}$ in H and 285 $\mathrm{A/m^2}$ in D, a co-extracted electron current fraction < 0.5 for H^- and < 1 for D^-, a beam current density uniformity better than 10% over the beam cross section and divergence in the range 3-7 mrad (e-folding) at 1 MeV. This last parameter is a quite strict requirement to fulfill in order to maximize the transmission of the HNB towards the tokamak and avoid heat load on beam line components. An important step towards the production of high current negative ion beams for fusion has been recently achieved at the Neutral Beam Test Facility (NBTF) in Padova, Italy. Starting from April 2021, the full-scale negative ion source of ITER Heating Neutral Beam injector, SPIDER, has been operated with Cs evaporation. When Cs is evaporated onto the source walls, surface assisted processes lead to a considerable increase of the extracted negative ion current and to an improvement of beam optics. SPIDER is an intermediate step towards the development of MITICA, the full-scale ITER HNB injector prototype, including the neutralizer and other beam components. The general technological and scientific targets of SPIDER are investigating and optimizing the source plasma, maximizing the negative ion current density, improving the beam current uniformity and studying the optics of the extracted negative ion beam up to an energy of 100 keV, i.e. the highest acceleration achievable in SPIDER. To monitor the extracted $\mathrm{H}^-/\mathrm{D}^-$ beam, SPIDER is equipped with a full set of diagnostics [2], in particular: a diagnostic equipped with IR cameras [3], visible cameras [4], an emittance scanner [5], single beamlet current sensors [6] and Beam Emission Spectroscopy (BES) [7], [8]. These techniques, when combined together, provide a detailed space and time resolution of beam properties during the entire plasma pulses and across the extraction area. BES consists in the analysis of the spectrum emitted by H/D atoms excited due to collisions of the $\mathrm{H}^-/\mathrm{D}^-$ beam with the residual $\mathrm{H}_2/\mathrm{D}_2$ gas downstream the beam acceleration system. A typical spectrum collected in a hydrogen plasma in SPIDER is shown in Fig. 1 and features a peak at the H_α emission wavelength, due to the atoms at rest, a Doppler shifted peak due to the excited atoms coming from the H^- beam and a stripping loss component due to negative ions neutralized before full acceleration. The Doppler shifted peak is due to the collection of photons with a Doppler shifted wavelength along the observation direction. For a single collected photon, its wavelength λ is given by:

$$\lambda = \lambda_0 \frac{1 - \beta \cos\alpha}{\sqrt{1-\beta^2}} \tag{1}$$

where λ_0 is the H_α / D_α wavelength, $\beta = v/c$ (with v the $\mathrm{H}^-/\mathrm{D}^-$ velocity), and α is the angle between the beam particles' trajectory and the direction of the collected photon.

The shape of the Doppler peak is the result of several instrumental effects such as the broadening introduced by the spectrometer (slit aperture width), the intrinsic H_α/D_α linewidth, the angular spread introduced by the finite dimensions of the collection optics and the fluctuations of the

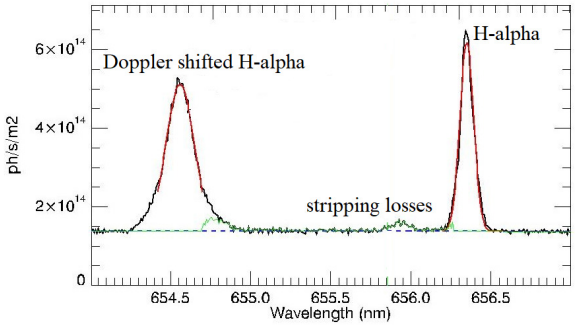

Fig. 1. Typical spectrum collected by the BES diagnostic in SPIDER for a beam extracted with 5 kV extraction and 45 kV acceleration. Source parameters were a source pressure of 0.33 Pa and 400 kW total RF power delivered to plasma.

R. Agnello is with Ecole Polytechnique Fédérale de Lausanne (EPFL), Swiss Plasma Center (SPC), CH-1015 Lausanne, Switzerland.

M. Barbisan, R. Pasqualotto and G. Serianni are with Consorzio RFX, Corso Stati Uniti 4, 35127 Padova, Italy.

G. Casati is with Imperial College London, Exhibition Rd., South Kensington, SW7 2BX, London UK.

acceleration voltage. [8] These contributions are subtracted for the estimate of the beamlet divergence, as detailed in Ref. [7] Furthermore, the asymmetry of the Doppler peak due to the finite size of the interaction volume, the variation of the size of the LOS cross section and the origin position of photons emitted in the detected volume are negligible, making a one-Gaussian fit well suitable. [9]

The divergence of single beamlets is directly related to the shape of the meniscus, the collection area of ions from the plasma in front of the plasma grid apertures. Particles with large velocity angles form the so-called *beam halo* and their mitigation is essential to minimize power losses along the beam transmission line. A common quantity in beam extraction physics is the *perveance* P, which is related to the extracted ion current I_{ion} and the extraction voltage V_{ext} by:

$$P = \frac{I_{ion}}{V_{ext}^{3/2}}. \tag{2}$$

The value of P for which the beam has its minimum divergence is defined as *perveance matching* condition. In the specific case of cylindrical symmetry, the maximum perveance allowed by the Child-Langmuir law reads:

$$P_0 = \frac{4}{9}\pi\epsilon_0\sqrt{\frac{2q}{m_{ion}}}\left(\frac{r}{d}\right)^2, \tag{3}$$

where m_{ion} is the ion mass, q the species charge, r the radius of the extraction aperture, and d the width of the extraction gap. In the case of SPIDER, $r = 7\,\mathrm{mm}$ and $d = 5.6\,\mathrm{mm}$. To compare the extraction capabilities among different extraction systems and ion species, the beam divergence is often plotted as a function of the *normalized perveance*, given by P/P_0.

II. EXPERIMENTAL SETUP

The extraction of negative ions in SPIDER is based on a three grid system, each featured by 1280 apertures from which approximately cylindrical beamlets are extracted [10]. Starting from the plasma side these are denoted as: plasma grid (PG), at about the source voltage which can be biased with respect to the source walls to reduce the co-extracted electrons; 2) extraction grid (EG), which can be biased from 0.4 to 12 kV, in which permanent magnets are embedded to suppress co-extracted electrons, and 3) a grounded grid (GG), biased from 20 to 100 kV, from which negative ion beamlets exit. The voltage applied between the gaps PG-EG and EG-GG are respectively denoted with V_{ext} and V_{acc}. An additional frame, the *bias plate*, located at 10 mm from the PG surface, can be biased with respect to the source walls reducing the amount of co-extracted electrons. Fig. 2 shows a schematic of a vertical cross section for a single extraction aperture. The acceleration of negative ions is therefore performed between two gaps. The stripping loss peak visible in Fig. 1 at 655.9 nm is mainly due to negative ions stripped in the PG-EG gap. Fig. 3 shows a schematic of the currently available extracted beamlets (yellow dots) and the position of BES LOSs. For both horizontal and vertical LOSs $\alpha = 75°$.

The GG is separated in 4 segments, numbered from top. Only 28 out of the 1280 apertures were available during

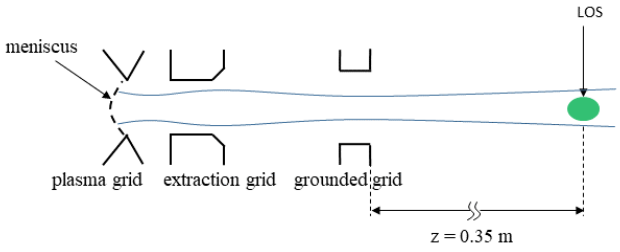

Fig. 2. Schematic of the three-grid extraction system and the beamlet profile.

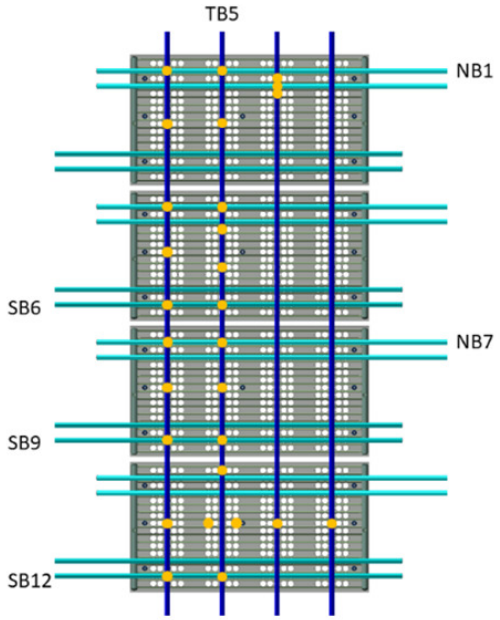

Fig. 3. Position of the lines of sight available for BES and the extracted beamlets (yellow dots) exiting the grounded grid seen from downstream.

the 2021 experimental campaigns, due to a mask installed on the downstream side of the PG. The mask was required to minimize gas conductance between the source and the vessel while waiting for an improvement of the pumping system during the experimental shutdown following this first Cs operations. Due to the few available beamlets, the exposure time of the spectrometer is 4.7 s and acquisitions are repeated every 5 s. In order to compare LOSs with maximum signal-to-noise ratio and with similar interaction geometries with beamlets, only horizontal LOSs with labels NB1, SB6, NB7, SB9, SB12 are taken into account because they are centered with extraction apertures. The only available vertical LOS, TB5, however, even though it is aligned with the extraction apertures, the beamlets are horizontally displaced by the criss-cross deflection due to compensation magnets embedded in the EG [11]. Although limiting the total extracted ion current and therefore the signal received by BES, this configuration of available beamlets is suitable to perform beam optics measurements on the scale of the single beamlet and to compare with single beamlet numerical simulations [12].

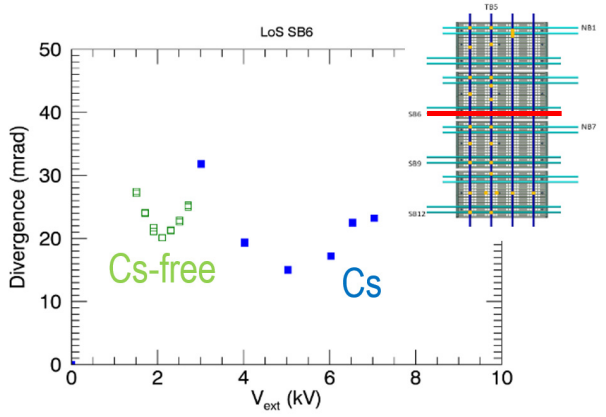

Fig. 4. Comparison of extraction voltage scans performed in Cs-free and Cs with the same RF power of 400 kW. For the Cs-free scan: $V_{acc} = 20\,\mathrm{kV}$, $I_{pg} = 1.5\,\mathrm{kA}$ (reversed). For the Cs scan: $V_{acc} = 45\,\mathrm{kV}$, $I_{pg} = 1.5\,\mathrm{kA}$.

III. DISCUSSION OF THE RESULTS

To quantify the effect of Cs evaporation on beam optics, two optics scans with similar source and extraction parameters but with and without Cs are compared. These data can be also cross checked with other diagnostics. For similar source and extraction parameters, electrical measurements detected an increase of the extracted negative ion current (a factor 3-4) and a considerable reduction of the co-extracted electron fraction (about a factor 10) with Cs. Fig. 4 shows two V_{ext} scans performed at a vertically centered line-of-sight (SB6), with the same total RF power of 400 kW delivered to plasma in Cs-free and Cs conditions. These trends exhibit a parabola-like shape, whose minima V_{ext}^{min} can be correlated with the optimal j_{ext} by the Child-Langmuir relationship [13]:

$$V_{ext}^{min} = V_{ext,0}^{min}\left(\frac{j_{ext}}{j_{ext,0}}\right)^{2/3} \tag{4}$$

where $V_{ext,0}^{min}$ is the value of V_{ext} where divergence is minimum for the nominal extracted current. The increase of extracted negative ion current density from 15 to 55 $\mathrm{A/m^2}$, deduced by electrical measurements, is compatible with the displacement of the perveance matching from 2.0 to 5.0 kV. Also, we observe that the optimum beam optics is obtained for a ratio V_{acc}/V_{ext} of about 9.5, as expected by beam transport simulations during the design of SPIDER accelerator [10]. The transition from the Cs-free to the Cs condition is also observed by other LOSs.

Although with the present configuration with only a few beamlets a spatially resolved characterization of the beam is difficult, it is anyway possible to compare single rows of beamlets for different grounded grid segments. Fig. 5 shows extraction voltage scans observed by all analysed horizontal and one vertical LOS. Compared to Cs-free operations, a overall decrease of divergence and the general approaching to the ITER target of 7 mrad is observed. The divergence minima are spread over the V_{ext} range, suggesting different extracted ion current densities, and, therefore, a non-uniform density of negative ions in front of the PG extraction apertures. The cause of this vertical inhomogeneity is, for example, due to

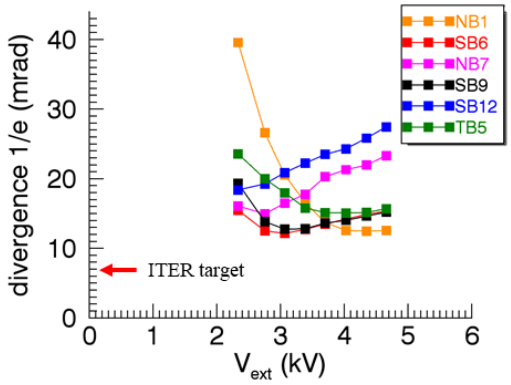

Fig. 5. Extraction voltage scans measured by 5 horizontal and 1 vertical LOS showing beam vertical inhomogeneity. Source and extraction parameters are 180 kW RF power, $V_{acc}/V_{ext} = 9.5$, $I_{pg} = 1.2\,\mathrm{kA}$.

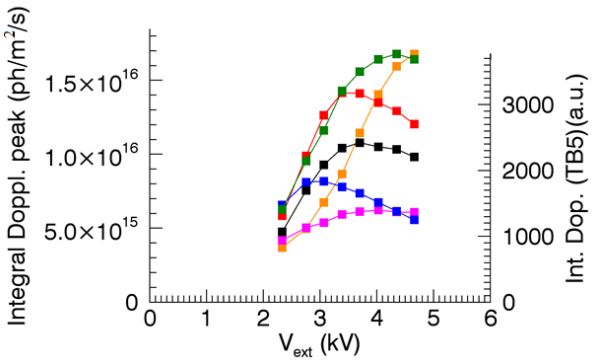

Fig. 6. Doppler peak integrals trends follow the respective beamlet divergences in the opposite direction. Source and extraction parameters are 180 kW RF power, $V_{acc}/V_{ext} = 9.5$, $I_{pg} = 1.2\,\mathrm{kA}$.

the localised RF power deposition from ICP drivers across the plasma cross section, the uneven Cs surface distribution and the $\vec{E}\times\vec{B}$ drift. In SPIDER, in the standard configuration of biased PG and bias plate and I_{pg} flowing towards the bottom, the highest plasma density is observed at the uppermost segment.

Together with the divergences, we show the corresponding values of the integral of Doppler shifted peak distribution over wavelength (in Fig. 6), which we will refer to *Doppler peak integral* in the following text. These are opposite to the trends of divergence. This suggests that despite the overall increase of extracted ion current, which was about 20% in this specific shot, as the beamlets divergence increases, the number of photons collected from the detection volume decreases. From the experimental point of view, the knowledge of beam divergence and intensity measured by BES and other beam techniques guided the source operators to properly balance machine parameters, for example by tuning the RF power for each power generator, to improve RF power deposition and, consequently, beam current vertical homogeneity. By comparing the Doppler peak integrals at different LOSs, it was remarked that the increase of the Cs injection rate from

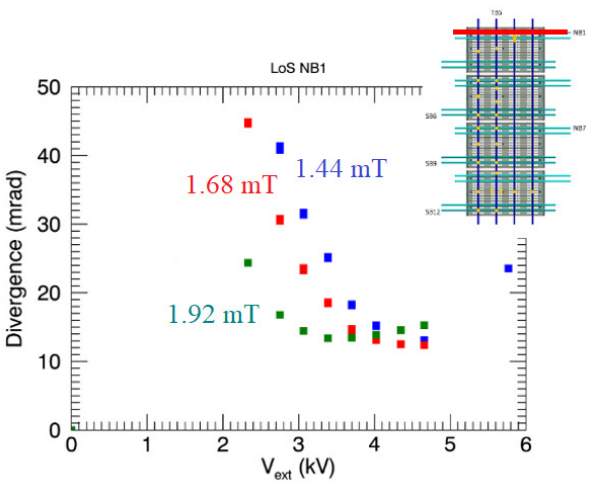

Fig. 7. Beam optics scans with $V_{acc}/V_{ext} = 9.5$ and three values of magnetic filter field intensity, for the pair of beamlets located at the top of segment 1 (NB1). Total delivered RF power to plasma is 180 kW and $p = 0.4\,\mathrm{Pa}$ source pressure.

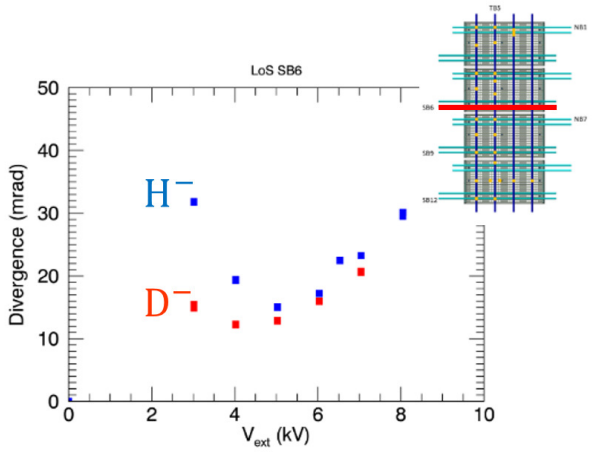

Fig. 8. Beam optics scans in hydrogen and deuterium with 400 kW total delivered power to plasma and $I_{pg} = 1.5\,\mathrm{kA}$. The acceleration voltages are $V_{acc} = 45\,\mathrm{kV}$ in hydrogen and $V_{acc} = 40\,\mathrm{kV}$ in deuterium.

6 to 24 mg/h is beneficial for beam uniformity [14].

Among the other machine parameters, one having an important effect on negative ion extraction is the magnetic filter field. Although it is helpful to reduce the neutralization processes of negative ions in the plasma, it can be detrimental to the symmetry of ion current density across the meniscus surface. Indeed, because of the combination of the filter field and the magnetic field produced by permanent magnets embedded in the EG, negative ions are transported along the horizontal direction, leading to a non-radially uniform negative ion current passing through the plasma meniscus [15]. These asymmetries introduced by the magnetic field in the extraction region break the cylindrical symmetry of beamlets and, eventually, lead to asymmetric Doppler peaks. The effect of this phenomenon on BES spectra would deserve a dedicated study. Here we are interested in the global effect of the magnetic filter field because it can be easily controlled. Fig. 7 shows beam optics scans for three values of the magnetic filter field for the pair of beamlets located at the top of segment 1 (LOS NB1). The coefficient between the magnetic filter field in the proximity of the PG and the I_{pg} current is 1.6 mT/kA [16]. Similar trends are observed across the entire extraction area. The total delivered RF power to plasma is 180 kW and source pressure is 0.4 Pa. We observe that, as the filter field is increased, the minimum of the divergence shifts towards lower V_{ext}, therefore suggesting a reduction of the negative ion current density. It has been verified that the shift of the position of the minimum of divergence (from 4.6 to 3.3 kV) is compatible with the variation of the extracted negative ion current (from 13.4 to 8.4 mA) measured by a Hall current probe on one of the two beamlets located at the top of segment 1 [6], therefore providing direct comparison with BES.

In the very last part of this Cs experimental campaign, extraction with deuterium was tested. Extraction of negative ions in deuterium is more challenging than hydrogen mostly due to the larger amount of co-extracted electrons, which was about a factor 3 higher for similar source parameters. The larger co-extracted electron current in deuterium was already investigated in similar negative ion sources [17], [18], [19], [20], [21], [22], and it is very likely linked to the slower velocity of D^- ions due to their larger mass, leading to an increase of electron density in the region close to the PG. [23], [19] The extracted ion current in deuterium is about 30% less than hydrogen. In Fig. 8 we compare two V_{ext} scans at full available total power of 400 kW and similar source/extraction parameters for hydrogen and deuterium plasmas. We remark that deuterium beamlets are slightly less divergent, about 2 mrad less than hydrogen. Also, the minimum is shifted at lower extraction voltage, therefore less extracted ion current, which is coherent with electrical measurements on the Acceleration Grid Power Supply (AGPS). Although the difference in ion temperature between H^- and D^- ions close to extraction aperture might play a role in the beamlet divergence, it is more likely that the difference in the divergence minima between the two isotopes is mostly due to the difference in negative ion density in front of the PG. This hypothesis is supported by direct $\mathrm{H}^-/\mathrm{D}^-$ measurements by Cavity Ring-Down Spectroscopy and Optical Emission Spectroscopy. The difference of mobility and diffusion coefficient between the two isotopes might play an important role in the final distribution of negative ions in front of the plasma grid. To fully understand beamlets optics difference between hydrogen and deuterium, 3D meniscus simulations would be required.

Apart from the parametric scans, an interesting feature observed by BES starting from Cs operation is that the Doppler shifted peak shows long tails such as that shown in Fig. 9 which are an indication of the presence of a broad beam component. These particles with large transverse velocity represent the beam halo; their relative amount is defined as beam *halo fraction*. For the sake of simplicity we will only discuss the case of horizontal LOSs since the Doppler peak observed by the only available vertical LOS (TB5) would mix the contribution of the broad components coming from 11 beamlets, which might considerably differ from each other.

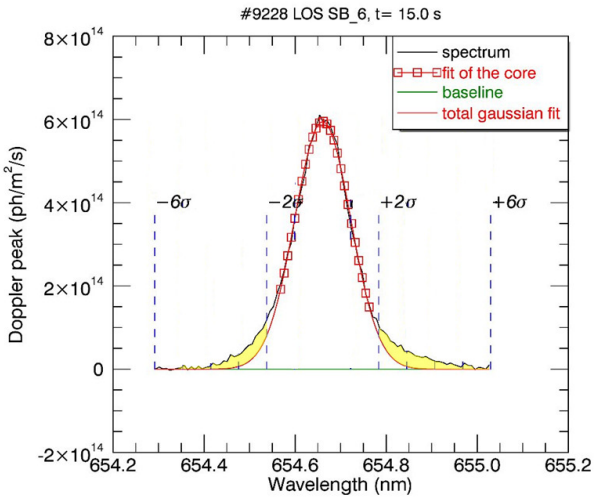

Fig. 9. Doppler shifted peak showing the presence of a broad component. A threshold at about 30% of the peak value has been applied to isolate the central core component from the large tails of the broad component. The highlighted area represents the amount of particles constituting the beam broad component. Source and beam parameters are: 180 kW total RF power delivered to plasma, $I_{pg} = 1.05\,\mathrm{kA}$, source pressure 0.35 Pa, extraction voltage $V_{ext} = 2.74\,\mathrm{kV}$, acceleration voltage $V_{acc} = 26.6\,\mathrm{kV}$.

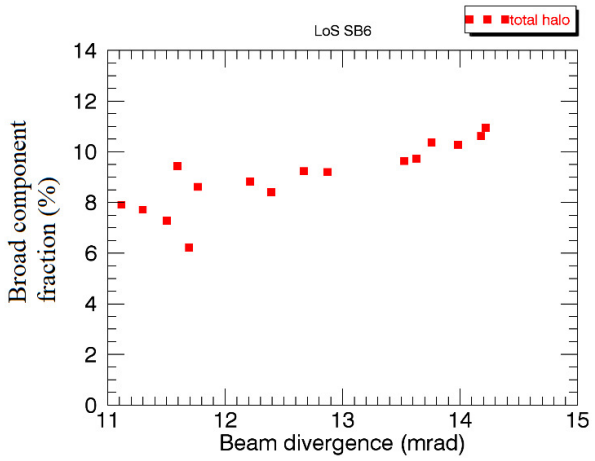

Fig. 10. The broad component fraction increases with the beam (narrow component) divergence, a trend coherent with the worsening of beam optics. Source and extraction parameters are 180 kW RF power, source pressure 0.35 Pa, $V_{acc}/V_{ext} = 9.5$, $I_{pg} = 1.05\,\mathrm{kA}$.

In order to quantify the broad component, a threshold of 30% of the Doppler peak has been applied, which seems to be a reasonable compromise, considering all the spectra. This threshold identifies the spectral range used to fit the beamlet narrow component. While the width of the Gaussian fit of the narrow component is used to evaluate the single beamlet divergence, the broad component can be interpreted as one or more populations of negative ions with larger transverse velocity component. Depending on the physical interpretation and the fitting methods, the broad component fraction can considerably vary and could represent an important fraction of the overall beamlet velocity population [9]. Since the physical mechanisms leading to the production of populations of negative ions with different temperatures are not well understood, we adopt here a more simple and pragmatic approach. As depicted in Fig. 9, the broad component fraction is estimated as the difference area between the measured spectrum and the Gaussian fit of the core component in a given spectral range (yellow highlighted areas), and normalized to the total Doppler peak integral. For the following analysis the integration range has been chosen between $\pm 2\sigma$ and $\pm 6\sigma$ of the narrow Gaussian fit curve. This provides an estimate of the relative excess of particles having high transverse component, compared with the expectations from a pure Gaussian beam. Preliminary estimates performed with this method provides a broad component fraction of the order of 6-11% in typical extraction voltage scans. The beam broad component has to be carefully monitored in ITER HNB injectors to avoid power losses on the beamline components, and it should not be higher that 15% [9]. Although our estimate of the broad component regards the velocity rather than the physical space, these preliminary results would confirm that, at least for these low-power experimental campaigns, the relative amount of the beam halo fullfills ITER requirements. The origin of this halo fraction is currently debated: negative ions with large velocity angles are likely to be originated from the edge of the meniscus [24], [25], [26]. Another possible origin of negative ions with large transverse trajectories might be due to negative ions originating from the downstream side of the PG apertures [27]. If this is the case, this would mean that part of Cs could migrate downstream and this could represent an issue to be carefully monitored, since Cs deposition on the beam duct can cause high voltage holding problems.

To investigate the amount of unfocused particles as beam optics varies, the broad component fraction as a function of the beamlet divergence is shown. Fig. 10 shows the broad component fraction observed by the LOS SB6 as a function of the beamlet (narrow component) divergence, showing a linear correlation. This is coherent with the fact that as beam divergence increases, the overall beam optics worsens. Similar trends are observed at other LOSs. The next envisaged step to support the interpretation of the broad component is running a code simulating BES spectra starting from the emission of beamlets with current density profiles, including a halo component. This might contribute to provide further insights on the physics of SPIDER negative ion beamlets.

IV. SUMMARY

One of the crucial parameters to be optimized in the development of HNB injectors is the negative ion beam divergence. First operations of SPIDER in Cs consisted in the extraction of well spatially separated beamlets making it possible for BES to characterize almost single beamlets. In particular, the improvement of beam optics from pure volume to Cs production of H^- was verified, the effect of the magnetic filter field on beam optics scans was studied, first D^- beamlet optics scans were shown, and, beam uniformity across the extraction areas was discussed. Furthermore, preliminary estimates of the broad component fraction show that, at perveance matching, ions with large velocity angle represent less than 10% of the

beamlet.

For future SPIDER operations, it is expected that the increase of RF power delivered to plasma will lead to an increase of the total extracted ion current, as well as to the co-extracted electron current. Concerning the ITER divergence target of 7 mrad, it is unfortunately not immediate to extrapolate the beam characteristics at full power (800 kW) and acceleration voltage (100 kV) operations on the basis on the low power/acceleration experiments discussed in this contribution. In general, the experience acquired in SPIDER operation is crucial to learn how to address the technical issues that will be inevitably encountered while operating MITICA.

Once accomplished the RF and pumping system replacement during the shutdown, preliminary experiments will be dedicated to the assessment of the new RF equipment, testing the new pumping system during 1h pulses, then, efforts will be devoted to optimize beam optics. The improvement of the pumping system is also expected to provide the pumping speed required to the extraction of the 1280 beamlets, therefore approaching to the source HNB requirement of a negative ion beam extracted across the entire grounded grid surface. To summarize, these results pave the way for further and detailed beam studies once the source will reach full extraction capabilities.

V. ACKNOWLEDGMENTS

This work has been carried out within the framework of the EUROfusion Consortium, funded by the European Union via the Euratom Research and Training Programme (Grant Agreement No 101052200 — EUROfusion). Views and opinions expressed are however those of the author(s) only and do not necessarily reflect those of the European Union or the European Commission. Neither the European Union nor the European Commission can be held responsible for them. This work has been carried out within the framework of the ITER-RFX Neutral Beam Testing Facility (NBTF) Agreement and has received funding from the ITER Organization. The views and opinions expressed herein do not necessarily reflect those of the ITER Organization. This work was supported in part by the Swiss National Science Foundation.

REFERENCES

[1] R. S. Hemsworth, D. Boilson, P. Blatchford, M. Dalla Palma, G. Chitarin, H.P.L. de Esch, F. Geli, M. Dremel, J. Graceffa, D. Marcuzzi, G. Serianni, M. Shah, D. Singh, M. Urbani, and P. Zaccaria. Overview of the design of the ITER heating neutral beam injectors. *New J. Phys,*, 19:025005, 2017.

[2] R. Pasqualotto, M. Agostini, M. Barbisan, M. Brombin, R. Cavazzana, G. Croci, M. Dalla Palma, R. S. Delogu, M. De Muri, and A. Muraro. A suite of diagnostics to validate and optimize the prototype ITER neutral beam injector. *Journal of Instrumentation*, 12:C10009, 2017.

[3] A. Pimazzoni, M. Brombin, G. Canocchi, R. S. Delogu, D. Fasolo, L. Franchin, B. Laterza, R. Pasqualotto, G. Serianni, and M. Tollin. Assessment of the SPIDER beam features by diagnostic calorimetry and thermography. *Rev. Sci. Instrum.*, 91:033301, 2020.

[4] M. Ugoletti, M. Agostini, M. Barbisan, M. Brombin, M. Cavenago, R. S. Delogu, F. Molon, R. Pasqualotto, A. Pimazzoni, and G. Serianni. Visible cameras as a non-invasive diagnostic to study negative ion beam properties. *Rev. Sci. Intrum.*, 92:043302, 2021.

[5] C. Poggi, E. Sartori, M. Tollin, B. Matteo, M. Zaupa, E. Fagotti, and G. Serianni. Design and development of an Allison type emittance scanner for the SPIDER ion source. *Rev. Sci. Instrum.*, 91:013328, 2020.

[6] A. Shepherd, T. Patton, A. Pimazzoni, B. Pouradier Duteil, A. Rigoni, E. Sartori, and G. Serianni. Initial results from the SPIDER beamlet current diagnostic. *in preparation*, 2022.

[7] M. Barbisan, B. Zaniol, R. Pasqualotto, G. Serianni, and M. Ugoletti. First results from beam emission spectroscopy in spider negative ion source. *Plasma Phys. Control. Fusion*, 63:125009, 2021.

[8] B. Zaniol, R. Pasqualotto, and M. Barbisan. Design of a beam emission spectroscopy diagnostic for negative ions radio frequency source SPIDER. *Rev. Sci. Intrum.*, 83:043117, 2012.

[9] F. Bonomo, M. Barbisan, U. Fantz, A. Hurlbatt, I. Mario, D. Wünderlich, and NNBI-Team. Overview of the beam physics investigation at the elise test facility. *AIP Conference Proceedings*, 2011:060011, 2018.

[10] P. Agostinetti, V. Antoni, M. Cavenago, G. Chitarin, N. Marconato, D. Marcuzzi, N. Pilan, G. Serianni, P. Sonato, P. Veltri, and P. Zaccaria. Physics and engineering design of the accelerator and electron dump for SPIDER. *Nucl. Fusion*, 51:063004, 2011.

[11] N. Marconato, G. Chitarin, P. Agostinetti, N. Pilan, and G. Serianni. Simulation, code benchmarking and optimization of the magnetic field configuration in a Negative Ion Accelerator. *Fusion Eng. Des.*, 86:925, 2011.

[12] G. Serianni, P. Agostinetti, V. Antoni, C. Baltador, M. Cavenago, G. Chitarin, N. Marconato, R. Pasqualotto, E. Sartori, V. Toigo, and P. Veltri. Numerical simulations of the first operational conditions of the negative ion test facility spider. *Rev. Sci. Instrum.*, 87:02B927, 2016.

[13] A. T. Forrester. *Large Ion Beams: Fundamentals of Generation and Propagation*. Wiley-Interscience, 1988.

[14] G. Serianni. Spatially-resolved diagnostics for optimisation of large ion beam sources. *in preparation*, 2022.

[15] S. Denizeau, D. Aprile, G. Fubiani, F. Taccogna, P. Minelli, M. Ichikawa, J. Hiratsuka, M. Kashiwagi, A. Kojima, and G. Chitarin. Experimental and numerical investigation on the asymmetry of the current density extracted through a plasma meniscus in negative ion accelerator. *Plasma Sources Sci. Tech.*, 29:075012, 2020.

[16] N. Marconato, M. Brombin, M. Pavei, M. Tollin, L. Baseggio, M. Fincato, L. Franchin, A. Maistrello, and G. Serianni. An optimized and flexible configuration for the magnetic filter in the spider experiment. *Fusion Engineering and Design*, 166:112281, 2021.

[17] D. Wünderlich, R. Riedl, I. Mario, U. Fantz, B. Heinemann, and W. Kraus. Formation of large negative deuterium ion beams at elise. *Rev. Sci. Intrum.*, 90:113304, 2019.

[18] S. Cristofaro, R. Friedl, and U. Fantz. Negative hydrogen and deuterium ion density in a low pressure plasma in front of a converter surface at different work functions. *Plasma*, 4:94–107, 2021.

[19] K. Ikeda, K. Tsumori, H. Nakano, M. Kisaki, K. Nagaoka, S. Kamio, Y. Fujiwara, Y. Haba, and M. Osakabe. Negative hydrogen and deuterium ion density in a low pressure plasma in front of a converter surface at different work functions. *Nucl. Fusion*, 59:076009, 2019.

[20] W. Kraus, D. Wünderlich, U. Fantz, B. Heinemann, F. Bonomo, and R. Riedl. *Rev. Sci. Instrum.*, 89:052102, 2018.

[21] R. Friedl and U. Fantz. Fundamental studies on the cs dynamics under ion source conditions. *Rev. Sci. Instrum.*, 85:02B109, 2014.

[22] U. Fantz, L. Schiesko, and D. Wünderlich. A comparison of hydrogen and deuterium plasmas in the ipp prototype ion source for fusion. *AIP Conference Proceedings*, 1515:187, 2013.

[23] M. Bacal and M. Wada. Deuterium results at the negative ion source test facility elise. *Plasma Sources Sci. Technol.*, 29:033031, 2020.

[24] S. Nishioka, K. Miyamoto, S. Okuda, I. Goto, A. Hatayama, and A. Fukano. Study of plasma meniscus and beam halo in negative ion sources using three dimension in real space and three dimension in velocity space particle in cell model. *Rev. Sci. Instrum.*, 85:02A737, 2014.

[25] K. Miyamoto, S. Okuda, A. Hatayama, M. Hanada, and A. Kojima. Study of beam optics and beam halo by integrated modeling of negative ion beams from plasma meniscus formation to beam acceleration. *Appl. Phys. Lett.*, 102:023512, 2013.

[26] I. M. Montellano, D. Wünderlich, S. Mochalskyy, and U. Fantz. 3D-PIC modelling of a low temperature plasma sheath with wall emission of negative particles and its application to NBI sources. *J. Phys. D: Appl. Phys.*, 52:235202, 2013.

[27] H.P.L. De Esch and L. Svensson. Negative ion beam halo mitigation at the 1MV testbed at IRFM. *Fusion Eng. Des.*, 86:363–368, 2011.